Development of a dynamic interferometric focusing system for femtosecond laser machining

Marcus Paulo Raele[1], Lucas Ramos De Pretto, Ricardo Elgul Samad, Anderson Zanardi de Freitas, Wagner de Rossi, Nilson Dias Vieira Junior and Niklaus Ursus Wetter.
Nuclear and Energy Research Institute, IPEN-CNEN/SP, Av. Prof. Lineu Prestes, 2242
Cidade Universitária – CEP 05508-000, São Paulo – SP – Brasil

ABSTRACT

Taking advantage of the inherent characteristics of femtosecond laser used for machining, we developed an interferometric system able to evaluate and correct the focal position with an accuracy of a few microns, implementing a technique based on low coherence interferometry. This approach measures at the exact spot that the laser is machining, in real time, and is sensitive to any sample that acts as a scatterer to the wavelength in use. The experimental evaluation was divided in two steps: in the first a system based on a superluminescent LED was mounted to check the viability and develop the controlling software; in the second part a setup was mounted employing a femtosecond laser, and several kinds of samples using the active focus control, among which the results obtained with glass sample and a bovine tooth are meticulously described in this paper. The system was able to improve the performance in both samples, keeping them in the confocal region for an extended positioning range, resulting in better engraving by the laser.

Keywords: femtosecond, machining, low coherence interferometry.

1. INTRODUCTION

One of the many applications of femtosecond laser pulses (FSP)[1] is micro-ablation and micro-machining[2]. The characteristics of an ultrashort pulse allow processing any type of material (metals, dielectrics, composites, biological tissues) with micrometric resolution without significant thermal deposition, in an extremely precise and delicate way. Possible applications are countless, but as an example we can mention: high precision machining[3], functionalization of surfaces[4], surgery for refractive correction[5], treatment for severe burns to skin[6], among many others.

In spite of the mentioned advantages, there are still some scientific and technological barriers to their implementation in a routine basis. One of them: a dynamic focal adjustment system, accurate and sensitive to various types of materials (metal, ceramic, biological).

The methodologies currently carried out in our laboratories, which certainly parallels in several other research centers in the world, are limited to samples almost entirely with an extremely flat profile, limiting the extent of machining studies with FSP samples that can be remodeled to present these characteristics. However there is a range of samples that cannot be polished, smoothed, rectified etc, as in the case of living structures such as leafs, shells and tissues, or inorganic samples where the surface has a feature that should not be removed, e.g. micro-textured cutting tool[7].

Thus, the ability to adjust to complex surfaces is required for the widespread use of femtosecond processing technology in production environments, where materials to be processed have a greater variety of shapes and surfaces.

Develop and test a system able to measure and correct the mismatch of the focal plane and the surface under machining using low coherence interferometry and evaluate its performance.

1.1 Laser ablation

The ablation process is driven by the fluence of the ultrashort pulses in use (energy per area, or $J \cdot cm^{-2}$). For a material to be ablated the fluence must overcome a certain value, known as "ablation threshold", below which the desired process doesn't take place. FPSs promote energy deposition on very short timescales, on the order of 10^{-14} s, reaching very high

[1] mpraele@ipen.br

Frontiers in Ultrafast Optics: Biomedical, Scientific, and Industrial Applications XVII, edited by Alexander Heisterkamp, Peter R. Herman, Michel Meunier, Roberto Osellame, Proc. of SPIE
Vol. 10094, 100940N · © 2017 SPIE · CCC code: 0277-786X/17/$18 · doi: 10.1117/12.2256559

peak intensities enough to ablate any material, whilst transferring minimal thermal load into regions adjacent to the area of interest.

These characteristics are important when it is desired that the material substrate under treatment doesn't undergo changes in its properties due to temperature rise or shockwaves resulting from very energetic laser pulses, which usually occurs with lasers with temporally longer pulses.

The ablation phenomenon, as already mentioned, is closely dependent on the intensity of the radiation, which in turn is associated with the laser focus spot size. Thus, a precise adjustment of the focus on the surface to be treated is required, since a small deviation from the focus position promotes an increase its diameter of the focus that ultimately increases the area quadratically, resulting in decreased intensity. This degrades the accuracy of machining, both laterally, considering that the focal area is greater, and axially, as material efficiency removal varies with intensity.

Following this line of thought, the capability (accuracy and productivity) of femtosecond laser machining for routine use is closely related to the monitoring and focus control on the surface to be processed. One of the crucial steps in preparation for a machining setup is overlapping of the focal plane with the surface to be machined as shown in Figure 1.

Considering a Gaussian beams[9], the matching overlap between the surface and the focus ideally occurs within the region *b*, called confocal zone, where the laser intensity can be considerate constant.

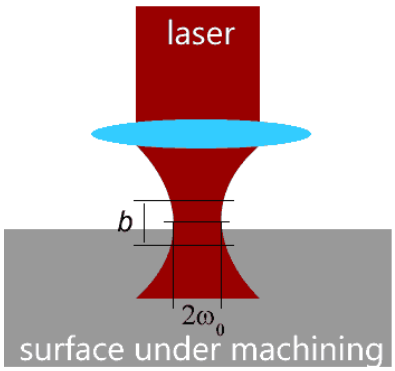

Figure 1: Laser focusing scheme.

As an example, using equations (1) and (2)[10] for the wavelength of a laser fs (Ti: Sapphire) with λ ~ 800 nm, a focalization lens with an effective focal length of 30 mm (*f*) and 10 mm beam diameter (*d*), results in a minimum focal diameter ($2\omega_0$) of 3 μm and confocal parameter 36 μm. In such hypothetical situation, ignoring the M^2 role for simplicity of this example, by positioning the sample surface 60 μm above or below the focal plane will double the focal diameter, reducing the laser intensity by a factor of 4, impairing the machining accuracy.

$$b = 8\frac{\lambda}{\pi}\left(\frac{f}{d}\right)^2 \tag{1}$$

$$2\omega_0 = \frac{4\lambda}{\pi}\left(\frac{f}{d}\right) \tag{2}$$

The overlap between the confocal region and the surface of the sample to be processed is difficult to adjust in practice, being usually performed nowadays through a series of laborious methods like engraving with the laser various marks on a sample and then evaluating the dimensions of these markings with the help of a microscope. This process, usually, takes up to an hour.

Commercial focus control systems are mostly based on capacitive systems, and therefore only work with metallic samples. Additionally, the system measures the position of the surfaces surrounding the beam, not directly at the point of machining. Such systems may be compatible with coarser and robust machining techniques, but when it comes to machining with FSPs this approach is flawed.

Although similar ideas are described in patents[11-12], no reports characterizing the proposed system was found in the scientific literature. Studies with different approaches were found, such as the one reported by Matthias *et al*. [13].

Therefore, the motivation of this work is to develop a method of monitoring and controlling the focus at the exact point of interest with high spatial precision, in real time, which is sensitive to any type of material.

1.2 Low Coherence Interferometry (LCI)

Among the most accurate approaches to assessment of dimensions and surface features are optical methods, most notably interferometric techniques, which are based on the wave nature of light in order to measure phase differences between different optical paths[14].

The interferometric techniques are mainly divided in two groups, namely coherent and incoherent interferometry, with the latter also referred to as low-coherence interferometry. Those approaches present notable differences in both: light source and light detection/analysis. The optical arrangement, however, does not change significantly and can be used under the same conditions for either purpose. An example of a widely used configuration is the Michelson interferometer, as presented in Figure 2.

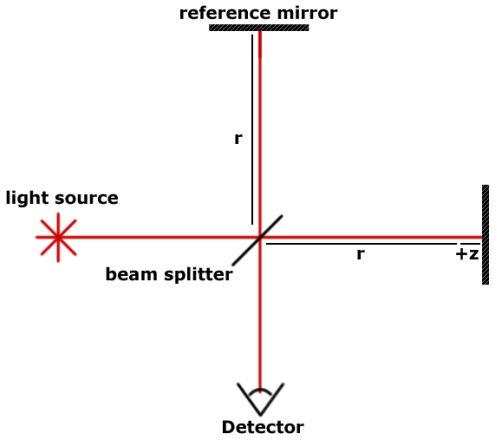

Figure 2: Michelson interferometer. The light source illuminates a beamsplitter The light travels through the arms of the interferometer and is reflected back toward the beamsplitter again, which overlaps the two beams and directs it to the detector.

The main difference between the high and low coherence techniques is that the former analyzes the interference between two monochromatic beams while the latter evaluates interferences between polychromatic beams. In practice and in summary, the first technique measures incremental displacements of the optical path difference (OPD) between arms and its precision is related to the wavelength used. The interferometric patterns occur for any OPD. Low coherence interferometry in turn univocally measures one OPD, i.e., there is a single interference pattern for each OPD. This becomes possible by evaluating the intensity oscillation as a function of wavelength. Analyzing the equation that describes the LCI intensity[15], one may reckon that it is proportional to a cosine as shown in equation (3), with I being the spectral intensity, k the wave number, n the refractive index and z the OPD. Such a term presents a frequency that is univocal for each z (for any $z > 0$) when analyzing a specific spectral region (i.e., as a function of k), and that's what enables the desired measurement.

$$I(k) \propto \cos(2knz) \qquad for \qquad z \geq 0, k = \frac{2\pi}{\lambda} \tag{3}$$

The resolution with which this OPD is measured is given by the coherence length, equation (4), where λ_0 is the central wavelength and $\Delta\lambda$ is the bandwidth measured at full width at half maximum (FWHM).

$$\Delta z = \frac{2\ln 2}{\pi}\frac{\lambda_0^2}{\Delta\lambda} \tag{4}$$

The LCI characteristics are, thus, ideal for determining the focal plane of a laser machining system. Moreover, the FSP used for machining usually have a bandwidth greater than 40 nm (Ti: Sapphire) resulting in, according to the equation (4), at least 6 μm resolution, enough to assess the focus position relative to the sample's surface. One may then intervene in the setup to keep the surface within the confocal region.

This study aims to develop, using spectral properties of the machining laser itself, an LCI system capable of measuring, with accuracy of a few micrometers and in real time, the focal position relative to the plane of interest, and making adjustments to maintain that surface within the confocal parameter of the focusing lens.

The idea is to complement the usual optical setup for machining, as in Figure 3a, obtaining a system that relies on an interferometer and a detection system as shown in Figure 3b.

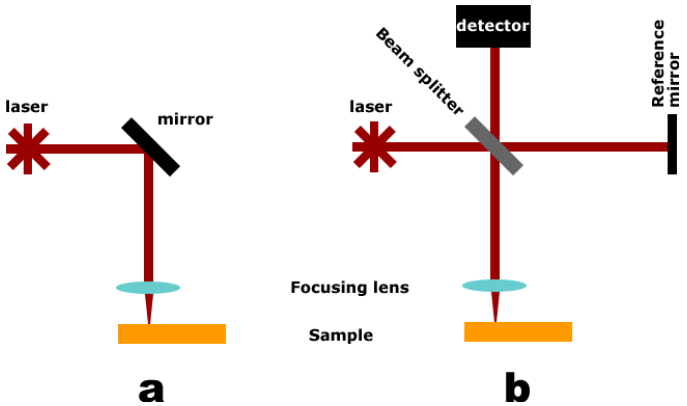

Figure 3: The difference between the optical setup of a regular laser machining station (a) and the proposed one (b).

For lasers with repetition rates of up to a few kHz, like chirped pulse amplification (CPA) systems, the interferogram analysis is easier when using the spectral approach, or Fourier Domain, for real time results. In this technique a spectrometer is used for detection, and after a computational treatment of the digitized signal one can retrieve information about differences between the optical paths of the interferometer arms.

It is worth emphasizing, however, that the focal position has no direct correlation with a given interferometric pattern. For the proposed application, it is necessary to determine the focal plane by means of the currently used method, and associate it with the generated interferogram. Nonetheless, this procedure is needed only once, for calibration of the system. Next the reference mirror will be locked, ensuring the situation illustrated in Figure 4, securing that the operator and the system always precisely know the mismatch of the focal plane and the surface under treatment. This procedure only needs to be repeated if the operator decides to changes the focusing lens.

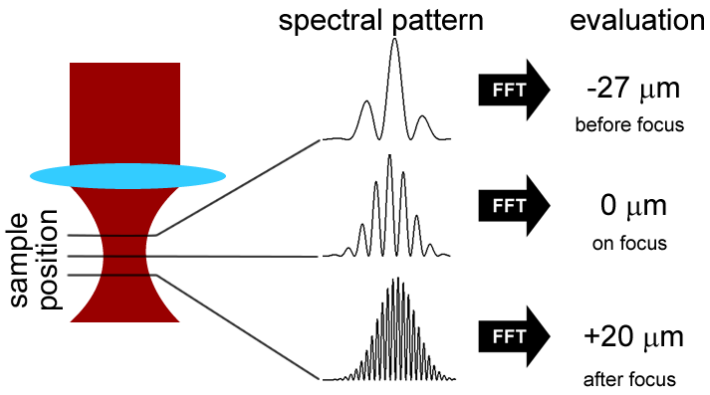

Figure 4: Illustration of the methodology of focus evaluation concept.

2. MATERIALS, METHODS & DISCUSSION

2.1 SLED setup

As a preliminary test, a setup using a super luminescent LED (SLED), instead of a femtosecond laser, was mounted to develop the basis of the controlling software, implemented in LabVIEW®, to pre evaluate the capabilities of the system. The technical specification of the main components are: SLED (Q-Photonics, model QSDM-830) pigtailed 2mW @195 mA centered at 831 nm; Spectrometer (OceanOptics, model USB4000) spectral range 599-898 nm blazed at 750 nm; Beamsplitter 50:50; 35 mm focusing lenses ; Translation stages (Thorlabs, model MTS25-Z8) mounted on a XZ configuration. Shown in Figure 5 are the details of the system configuration.

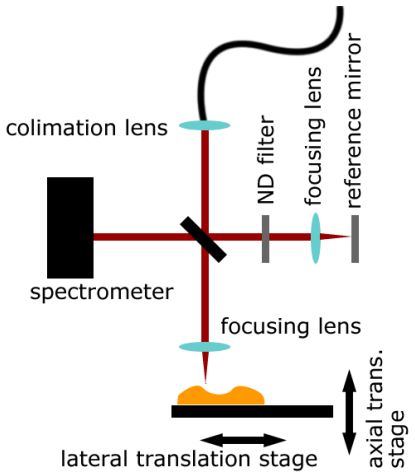

Figure 5: Schematic illustration of the setup.

The developed software acquires the information of the spectrometer and treats the data, following Equation 3 and performing the FFT, allowing the measurement of the surface's position, which appears as a peak in the treated signal is then located through second derivative analysis, and tracked via a developed algorithm. In every iteration during processing, the current scattering profile is analyzed and compared with a predetermined situation. Then the axial translation stage's position is adjusted whenever necessary. To prevent continuous movement around the ideal position, a

minimum mismatch parameter was implemented, avoiding correction for position differences below a certain threshold. The software operation is summarized in Figure 5.

Figure 6: Flow chart of controlling software working basis.

Using this system, several kinds of samples were tested, showing that the system is capable of laterally moving (raster) the sample, and gather interferometric information to continuously bring the sample to a fixed distance from the focusing lens. Metals and resins were tested with encouraging results. As an example, a coin of R$0.25 (25 cents of Brazilian Real), was roughly positioned on the stage, i.e., no procedure to level and tilt the sample took place. The system was able to perform both: surface (peak) location and axial correction. To evaluate the efficacy of the system these data was recorded to the same sample at the same path, with and without the dynamic focal correction and the results were compared. The results are displayed in Figure 7, showing the both situations.

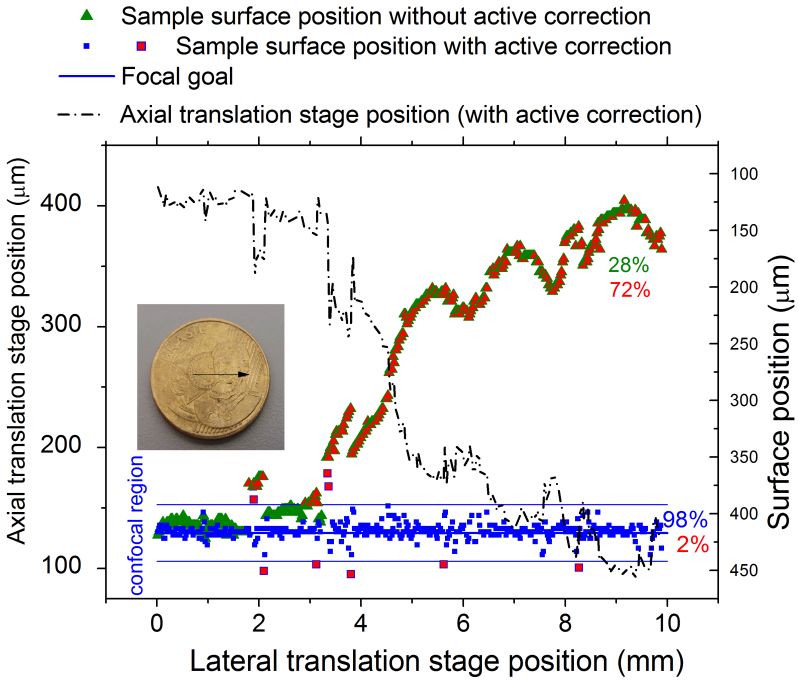

Figure 7: Comparison between applying (blue) or not the auto focusing system (green).

Green triangles show the surface position (peak detection) without correction as the lateral displacement occurs, solid green means they are within the confocal region, while red with green border, represent points out of the ideal region. For this case, only 28% of the machining would happen within the confocal region. With the active focusing, solid blue squares, 98% of the machining would take place within the confocal region. The red squares with blue border represent where the system could not correct properly. The dash & dot line, by its turn, shows the axial movement of the sample due to correction. It is interesting to note that this line complements the sample surface (green triangles) almost perfectly, as expected. In either way, actively correcting or not, it is possible to recover the sample's "profile plus tilt" with the LCI system developed. The tilt can be estimated fitting a straight line at the triangle data or the axial stage correction. The velocity of lateral scanning was 0.4 mm/s.

In this preliminary test, as the sample was not being ablated, it was possible to repeat the experiment over and over, refining the parameters and test situations, which contributed to the achieved 98% operation within the confocal region. Another aspect to highlight is that the SLED operates as a continuous wave (CW) light source with a smooth spectrum, characteristics that ease the interferometric analysis. Nonetheless, the preliminary system paved the way to the following step.

2.2 Femtosecond setup

The final setup counted with a femtosecond laser (Femtolasers, model Femtopower Compact Pro HP/HR) operating at 4 kHz, bandwidth of 40 nm centered at 785 nm. The only major modification at the optical setup, besides the light source, was the withdrawal of the focusing lens in the reference arm, as shown in Figure 8, aiming to avoid mirror damaging. For the motion control, another translation stage was added to access the vertical axis, enabling the system to scan over the entire sample's surface.

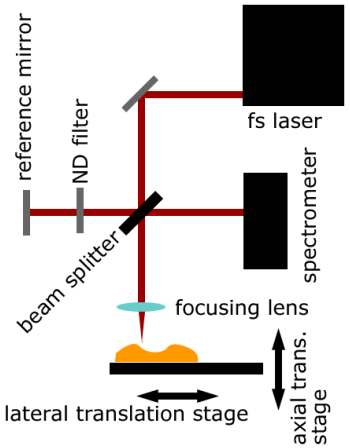

Figure 8: The schematic illustration of the final setup.

As mentioned in the introduction, the interferometric pattern has no direct correlation with the focal position, so it is necessary to stablish this relation, but this process needs to be performed just once. For this purpose, a microscope slide was used as a sample and then brought roughly into focal position. Analyzing the scattering profile (the FFT of the interferogram), the samples' tilt was corrected. A reference ruler was engraved (see Figure 9). Following, the laser energy was decreased to about 2 μJ, and the ruler was engraved again, but at this time the axial stage was continuously moved from a point before the focus to an end point after it, in steps of 20 μm, as illustrated at the left of Figure 9. With the help of a scanning electron microscope (Hitachi, model TM3000) it was possible to analyze the grooves closely, determine the optimal condition and recover the information about the most appropriated axial location.

The slide was placed at the setup again, at the calculated position, and the reference mirror was adjusted at an OPD arbitrary choose of 300 μm. In other words, if any surface peak was located by the interferometric system at a value smaller than 300 μm, the focus would be placed above the surface, while for values greater than 300 μm, the focus would be underneath the surface.

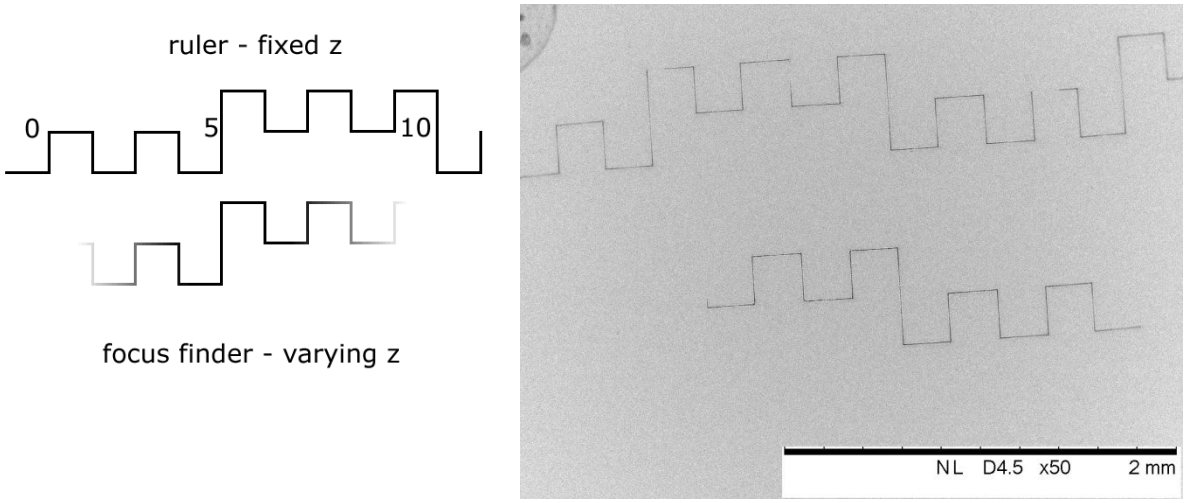

Figure 9: To find the focus, two patterns were engraved on a microscope slide. One was used as a ruler and the other was performed altering the position of the slide relative to the focusing lens, helping to find the focal plane.

The first tests were performed using a watch glass (commonly used in chemistry), which has the form of a spherical cap glass, see Figure 10. Grooves were successfully machined in a raster scan pattern at both, the convex and the concave sides. The a-scan (x axis) was set to travel for 20 mm at 0.75 mm/s, and the b-scan (y axis) consisted of 100 µm steps between lines, in a total of four. The pulse energy at the sample arm was 27 µJ, with ~50 fs of duration. The used focusing lens had 25 mm of focal length.

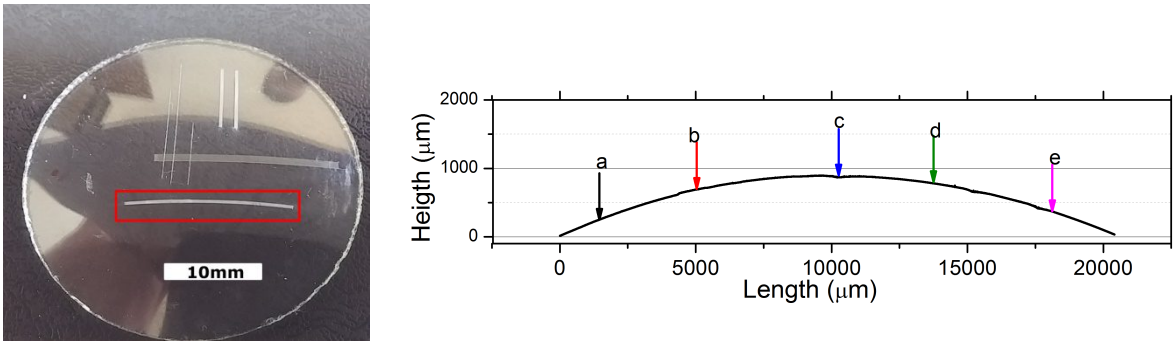

Figure 10: Watch glass used as sample, at left a photo showing the laser engraving under analysis (highlighted by a red border), at right, the measured profile of the engraved area. The arrows points where the groves were analyzed transversally.

The profile of the sample along the engraved region was recorded using a white light profilometer (Zygo, model Z-Gage), graphically represented in Figure 10 (right), showing the almost 1000 µm difference in height between the borders and the center of the engraved structures. Once again, neither previous leveling of the sample, nor any other aspect that could benefit the experiment somehow was performed.

The machining occurred at the region highlighted by the red square in the Figure 10, and data collected by the machining control software is exhibited in Figure 11, where one also have access to the information about the translation stage position[2]. The dash&dot line has a repetition pattern due to the raster going back and forth, see Figure 11 left. Such line

[2] To make the system faster, the absolute position gathered by inquiring the stage driver at the previous experiment was substituted by the incremental sum of corrections sent by the software to the driver, which may lead to the presence of cumulative errors due to rounding or which may arise from ignored commands due to the driver response limitation.

also stresses the sample tilting, noting that the raster starts with the axial position at 0 mm and finishes at about 3 mm. Also noteworthy is that 57% of the machining occurred within the confocal region. When considering that the sample plus the tilting summed ~3 mm of displacement and the confocal region was ~25 µm, it demonstrates the potential of the system even for an crude setup. Some peak detection outliers are also present. Working with a fs laser proved to be more defying than the SLED, mainly because of the variations on laser longitudinal modes, power and spectral drift added with low repetition rate, which hinders to dilute these variations. Typically, an integration time of 1 ms was used at the spectrometer, collecting few laser pulses, in this case only four.

The system proved to be more difficult to maintain the focus when the surface became steeper (at the borders) and when the lateral raster reversed the movement, causing a kind of overshoot error. For samples, such as this, with high relief amplitude, the system was not fast enough to keep the focusing within the confocal range during the entire procedure. Nevertheless, the system brought the focus back to the sample surface.

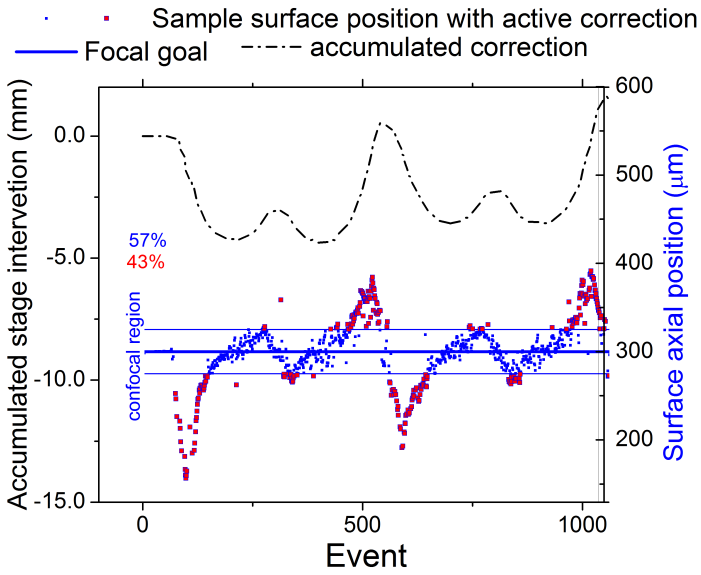

Figure 11: Surface position detection is represented by the scatter (right axis) Blue squares means within the confocal parameter, red squares with blue borders outside the region of interest. The dash&dot line shows the accumulated stage correction.

Machining uniformity: Using the profilometer the area of the machined region was measured (Figure 10), allowing to evaluate the characteristics of the channels machined at 5 different locations along the machining path, indicated by the colored arrows in Figure 10 (right). The grooves' transversal sections are shown in Figure 12 left.

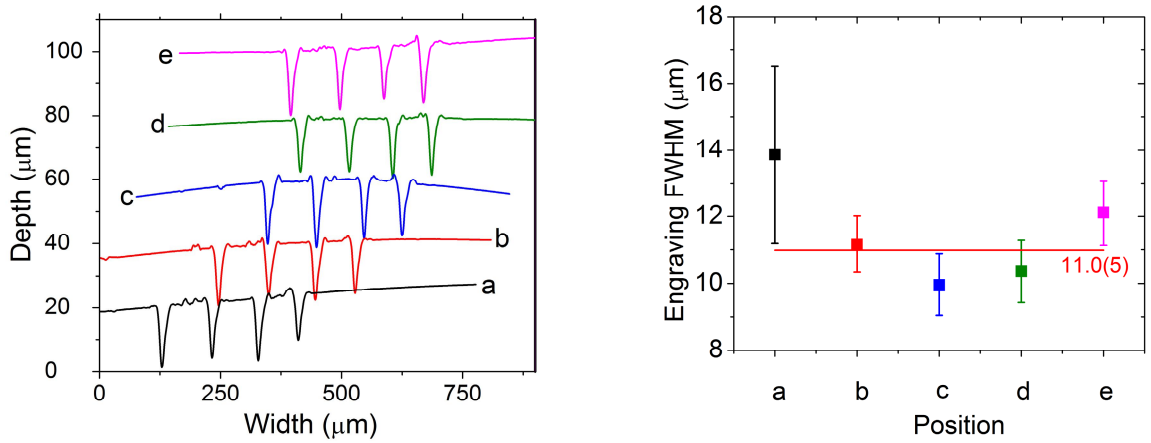

Figure 12: At left, the transversal section of the grooves at the positions indicated from (a) to (e) in Figure 10. At right the grooves FWHM and its weighted average.

Combining the information from the graphs of Figure 10 through Figure 12, it is possible to assess the overall performance of the system for this experiment. The system struggled to maintain the focus at the steeper region of the surface where the raster beginning is located. This difficulty is revealed by the FWHM bigger error bar (letter a). The grooves' shapes stabilize as the surface becomes flatter. At the beginning and end of the raster, as the stage accelerates and decelerates, the grooves width enlarges, in the middle (c in the x-axis) the stages are at full speed, causing a slightly thinner engraving. However all sets of grooves are very similar in depth and width. The Figure 12 right, shows in spite of the systems issues the FWHM was kept in certain agreement among them.

Finally a biological sample was also tested. A bovine tooth was machined and characterized. The laser energy was set to 9 μJ, the raster velocity to 0.5 mm/s, engraving two sets of 6 lines with 5 mm of length with and without the active control (for comparison purposes). The characterization also consisted in the profilometry of the regions where the laser acted. The ablated regions, along with their curvature (as measured by profilometry) are present in Figure 13. Worth to emphasizes that the area measured was a bit bigger than the machined region.

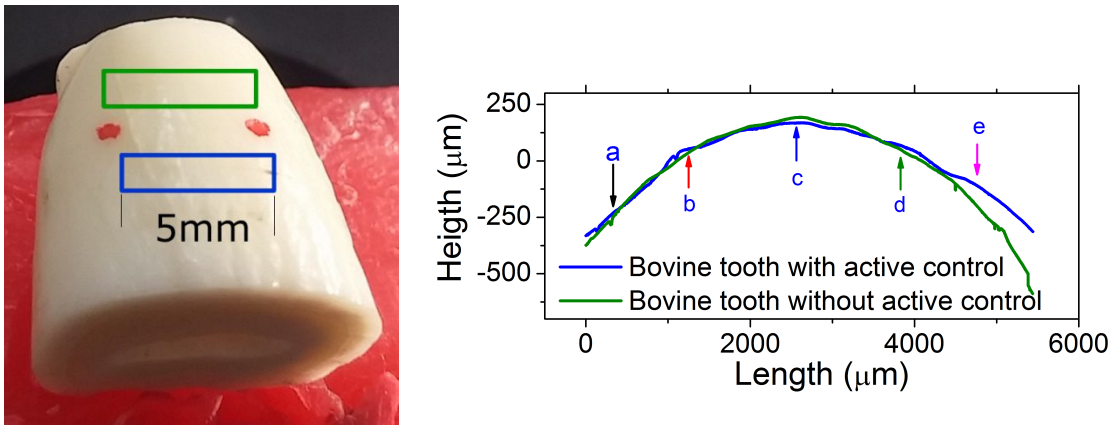

Figure 13: At left, the two machined regions, with active control bordered by blue, and without bordered by green. At right the surface, acquired by optical profilometry, using the same color codes.

The results of the machining with the active control are presented in Figure 14 (left). The graph exhibits the events in which the surface was in and out the confocal region, 56% and 44%, respectively, along ~200 μm total surface height variation. The system was able to cope with the sample along the 6 lines of raster. The main issue observed in this

experiment was due to the fact that the tooth is partially transparent to the wavelength applied, resulting in tomographic artifacts in the back scattered profile, i.e., the system also responds to inner structures of the sample, presented as peaks in the data, as occurs in optical coherence tomography technique (OCT) [15-16]. That eventually leaded to software misclassification of the true first surface, the one of interest. The overall appearance of the engraving, right of Figure 14, is constant throughout the ablation region.

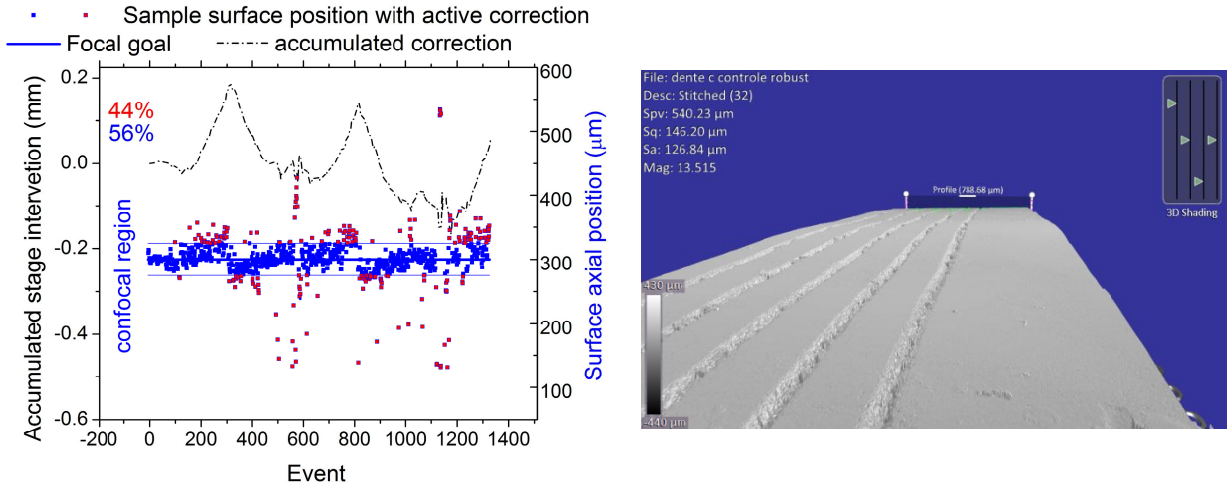

Figure 14: At left the surface position detection is represented by the squares (right axis), blue squares means within the confocal parameter, red squares with blue borders outside the region of interest. The dash&dotted line shows the accumulated stage correction. At right, the optical profilometer image, showing the engraving aspect on the bovine tooth.

Next, the same raster was performed without correction of the focal distance, in a region close to the one used in the first experiment. The system only collected information regarding the surface position, as seen in Figure 15. The curvature of this region was slightly steeper, however the system was able to track the surface in a substantial part of the experiment, and at the right of Figure 15, it is possible to observe the ablation processing ceasing due to the surface being far from the focal plane (located at ~3900 µm of the lateral axis).

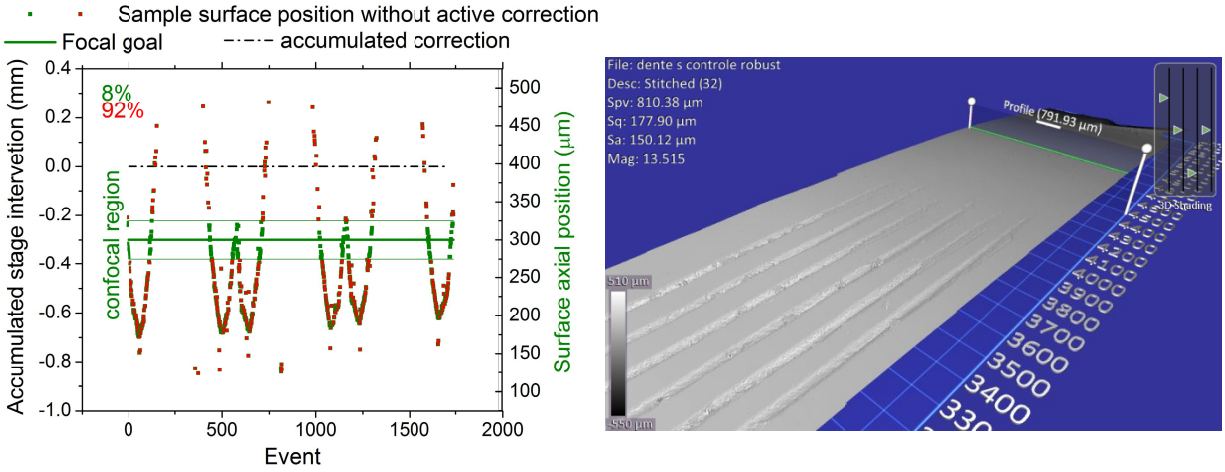

Figure 15: At left the surface position detection is represented by the scatter (right axis), green squares means within the confocal parameter, red squares with green borders outside the region of interest. The dash&dot line shows the accumulated stage correction. At right, the optical profilometer image, showing the engraving aspect on the bovine tooth.

For the groove width stability analysis, the same methodology applied as with the watch glass was performed, however it was done only for the engraving with the active focus control, since the other was not able to engrave an appreciable portion of the pattern. Figure 16 (left), shows the transversal sections of the engravings recorded at the locations pointed by the arrows in Figure 13, following the same color code and letters. Still in Figure 16 (right), the FWHM at each transversal cut is presented with its standard deviation (error bars) and its weighted average.
As the topography of the tooth presents almost a random profile, the variations in physical properties of the tooth bulk also have no strict regularity, in this way the grooves widths and its variation (size of the "error" bar) found at Figure 16 right, returned vague behavior pattern bringing few extra information besides that the system maintained, at these transversal sections, the focal position, being able to machining properly.

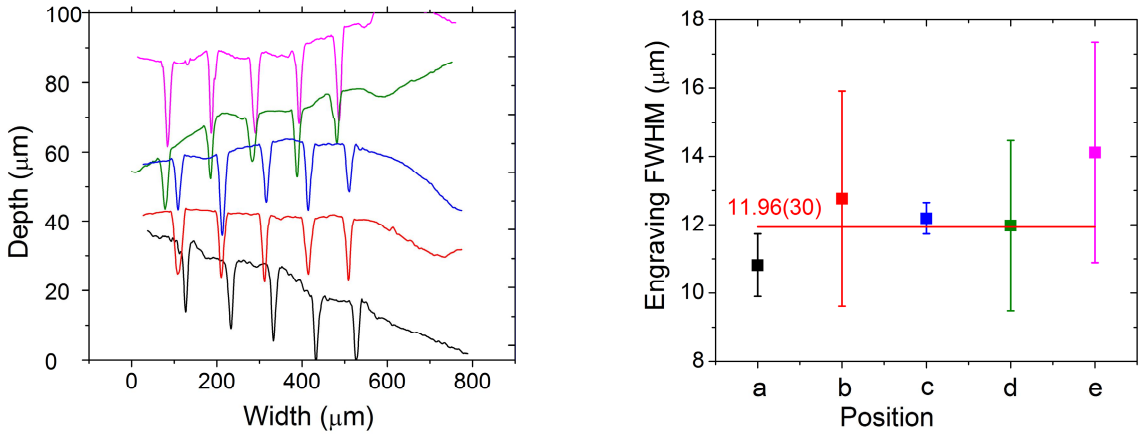

Figure 16: At left the transversal section of the grooves at the positions indicated from (a) to (e) at Figure 13. At right the grooves FWHM and its weighted average.

3. CONCLUSIONS

A system for dynamically maintain the focal plane over the surface under machining in real time was developed using low coherence interferometry and it was evaluated under several circumstances and criteria. The system is viable and proved to be able to cope with a great variety of materials and its optical peculiarities: the high reflectivity of metals, the high specular reflectivity of polished glass, the inner scatterings of biological samples are some examples tested.

The optical system has room for improvements though. Spectrometer collection, the reference beam attenuation, more appropriated machining lens are some aspects that deserves more attention to take the system one step closer to routine use. The main limitation however was found to be hardware communication, especially with the translation stages, slowing all the processing and interventions. With these issues, the software played a major role, having to be able to overcome the delayed information and actuation.

As the SLED setup raster was slower than the one with the FSP, the communication problems were not present, bringing the surface to the confocal region in about 98% of the total events. For the FSP setup, velocities up to 1 mm/s were achieved with the focal control, however this depended on the surface characteristics under machining. The velocities are low when compared with commercial laser processing stations, so the system needs further improvements to be able to substitute the system currently under use.

The grooves analyses demonstrated the importance of a control system such as the one developed when processing samples with no previous knowledge about the relief, even when the surface is predictable, as in the case with the watch glass, for instance. The system maintained the machined width stable along the raster, showing that it was able to keep the focal plane over the sample satisfactorily for the glass and the tooth, proving the efficacy of the proposed approach.

4. ACKNOWLEDGEMENTS

We thank the grant #2015/24878-0, São Paulo Research Foundation (FAPESP).

REFERENCES

[1] B. N. Chichkov, C. Momma, S. Nolte *et al.*, "Femtosecond, picosecond and nanosecond laser ablation of solids," Applied Physics a-Materials Science & Processing, 63(2), 109-115 (1996).

[2] R. E. Samad, L. M. Machado, N. D. Vieira Junior *et al.*, [Ultrashort Laser Pulses Machining] InTech, (2012).

[3] L. M. Machado, R. E. Samad, A. Z. Freitas *et al.*, "Microchannels Direct Machining using the Femtosecond Smooth Ablation Method," Lasers in Manufacturing 2011: Proceedings of the Sixth International Wlt Conference on Lasers in Manufacturing, Vol 12, Pt B, 12, 67-75 (2011).

[4] B. Wu, M. Zhou, J. Li *et al.*, "Superhydrophobic surfaces fabricated by microstructuring of stainless steel using a femtosecond laser," Applied Surface Science, 256(1), 61-66 (2009).

[5] R. Montes-Mico, A. Rodriguez-Galietero, and J. L. Alio, "Femtosecond laser versus mechanical keratome LASIK for myopia," Ophthalmology, 114(1), 62-68 (2007).

[6] M. O. Santos, W. Rossi, V. P. Goulart *et al.*, "FEMTOSECOND LASER HIGH INTENSITY IRRADIATION AS A PROPOSAL FOR ADJUVANT TREATMENT IN BURNED SKIN - AN IN VIVO MODEL," Lasers in Surgery and Medicine, 45, 31-31 (2013).

[7] T. Obikawa, A. Kamio, H. Takaoka *et al.*, "Micro-texture at the coated tool face for high performance cutting," International Journal of Machine Tools & Manufacture, 51(12), 966-972 (2011).

[8] S. Abdelli, [Capacitance height gauge] Google Patents, (1992).

[9] G. R. Fowles, [Introduction to Modern Optics] Dover-Publ., (1975).

[10] R. Osellame, G. Cerullo, and R. Ramponi, [Femtosecond Laser Micromachining: Photonic and Microfluidic Devices in Transparent Materials] Springer Berlin Heidelberg, (2012).

[11] B. Schürmann, and I. W. STORK, [Laser machining head with focus control] Google Patents, (2013).

[12] Y. C. Tseng, [Laser machining device] Google Patents, (2014).

[13] M. B, Z. M, B. D *et al.*, "Adaptive optics assisted and optical coherence tomography guided fs-laser system for ophthalmic surgery in the posterior eye," Journal of Biomedical Optics, 21(12), (2016).

[14] P. Hariharan, [Basics of Interferometry] Elsevier Science, (2010).

[15] A. Z. Freitas, M. M. Amaral, and M. P. Raele, [Optical Coherence Tomography: Development and Applications] InTech, Rijeka, 20 (2010).

[16] A. Z. Freitas, D. M. Zezell, N. D. Vieira *et al.*, "Imaging carious human dental tissue with optical coherence tomography," Journal of Applied Physics, 99(2), (2006).